Supporting Information

Visible-light-responsive hybrid photocatalysts for quantitative conversion of CO_2 to highly concentrated formate solutions

Ewan McQueen[a‡], Noritaka Sakakibara[b*‡], Kei Kamogawa[b], Martijn A. Zwijnenburg[c], Yusuke Tamaki[b], Osamu Ishitani[b,d*], and Reiner Sebastian Sprick[a*]

a. Department of Pure and Applied Chemistry, University of Strathclyde; Thomas Graham Building, 295 Cathedral Street, Glasgow G1 1XL, United Kingdom.

b. Department of Chemistry, School of Science, Tokyo Institute of Technology; 2-12-1-NE-2 Ookayama, Meguro, Tokyo 152-8550, Japan.

c. Department of Chemistry, University College London; 20 Gordon Street, London WC1H 0AJ, United Kingdom.

d. Department of Chemistry, Graduate School of Advanced Science and Engineering, Hiroshima University; 1-3-1 Kagamiyama, Higashi-Hiroshima, Hiroshima 739 8526, Japan

*Corresponding author. Email: nori.sakakibara@gmail.com; iosamu@hiroshima-u.ac.jp; sebastian.sprick@strath.ac.uk

‡These authors contributed equally to this work.

†Present address: Research Institute for Chemical Process Technology, Department of Materials and Chemistry, National Institute of Advanced Industrial Science and Technology (AIST), 4-2-1 Nigatake, Miyagino-Ku, Sendai, Miyagi 983-8551, Japan.

Procedures for the synthesis of the conjugated polymers

Synthesis of P1

1,4-Dibromobenzene (1.18 g, 5.0 mmol), 1,4-benzene diboronic acid (0.829 g, 5.0 mmol), tetrakis(triphenylphosphine)palladium(0) (38 mg, 0.7 mol%), *N*,*N'*-dimethylformamide (75 mL) and aqueous potassium carbonate solution (2.0 M, 15 mL) were added and refluxed at 150 °C under nitrogen for 72 hours. The mixture was then cooled to room temperature and poured into water (100 mL). The solid was collected by gravitational filtration and washed with MeOH. After a Soxhlet extraction with THF overnight, the product was obtained as a grey powder (588 mg, 77%).

Synthesis of P7

To a 100 mL two-necked round-bottomed flask, 1,4-dibromobenzene (235.9 mg, 1 mmol), 3,7-bis(4,4,5,5-tetramethyl-1,3,2-dioxaborolan-2-yl)dibenzo[*b*,*d*]thiophene sulfone (468.2 mg, 1 mmol) and potassium carbonate (691.0 mg, 5 mmol) were added with a stirring bar. The reagents were evacuated under vacuum and purged with nitrogen in three cycles. Tetrakis(triphenylphosphine)palladium(0) (3.46 mg, 0.0030 mmol, 0.3 mol%) was then added and the reagents were evacuated and purged three times as described above. Degassed *N*,*N'*-dimethylformamide (20 mL) and degassed water from a milli-Q water purification system (5 mL) was added. The mixture was left to stir and reflux at 150 °C under nitrogen for 72 hours. The mixture was then cooled to room temperature and poured into water (100 mL). The solid was collected by gravitational filtration and washed with MeOH. Further purification was performed by Soxhlet extraction overnight with $CHCl_3$ to extract low molecular weight byproducts. The solid product was dried under reduced pressure in a vacuum oven and obtained as a yellow powder (290.4 mg, 99%).

Synthesis of P10

To a 100 mL two-necked round-bottomed flask, 3,7-dibromodibenzo[*b*,*d*]thiophene sulfone (187.3 mg, 0.5 mmol), 3,7-bis(4,4,5,5-tetramethyl-1,3,2-dioxaborolan-2-yl)dibenzo[*b*,*d*]thiophene sulfone (234.0 mg, 0.5 mmol) and potassium carbonate (345.5 mg, 2.5 mmol) were added with a stirring bar. The reagents were evacuated under vacuum and purged with nitrogen in three cycles. Tetrakis(triphenylphosphine)palladium(0) (1.73 mg, 0.0015 mmol, 0.3 mol%) was then added and the reagents were evacuated and purged three times as described above. Degassed *N*,*N'*-dimethylformamide (10 mL) and degassed water from a milli-Q water purification system (2.5 mL) was added. The mixture was left to stir and reflux at 150 °C under nitrogen for 72 hours. The mixture was then cooled to room temperature and poured into water (100 mL). The solid was collected by gravitational filtration and washed with MeOH. Further purification was performed by Soxhlet extraction overnight with $CHCl_3$ to extract low molecular weight byproducts. The solid product was dried under reduced pressure in a vacuum oven and obtained as a yellow powder (169.1 mg, 78%).

Synthesis of P28

To a 100 mL two-necked round-bottomed flask, 2,5-dibromopyrazine (237.9 mg, 1 mmol), benzene-1,4-diboronic acid (165.8 mg, 1 mmol) and potassium carbonate (691.0 mg, 5 mmol) were added with a stirring bar. The reagents were evacuated under vacuum and purged with nitrogen in three cycles. Tetrakis(triphenylphosphine)palladium(0) (3.46 mg, 0.003 mmol, 0.3 mol%) was then added and the reagents were evacuated and purged three times as described above. Degassed *N*,*N'*-dimethylformamide (20 mL) and degassed water from a milli-Q water purification system (5 mL) was added. The mixture was left to stir and reflux at 150 °C under nitrogen for 72 hours. The mixture was then cooled to room temperature and poured into water (100 mL). The solid was collected by gravitational filtration and washed with MeOH. Further purification was performed by Soxhlet extraction overnight with $CHCl_3$ to extract low molecular weight byproducts. The solid product was dried under reduced pressure in a vacuum oven and obtained as a yellow powder (133.3 mg, 85%).

Details of the computational calculations

The ionization potential (IP) and electron affinity (EA) of the polymers in DMA were predicted by ΔDFT calculations following a previously developed approach.[1, 2] In this approach the polymer is described as a single polymer strand embedded in a continuum dielectric with the dielectric permittivity of the (major component of the) reaction mixture, here DMA (εr 37.8). The use of a continuum solvation model allows for the description of the dielectric screening of charges in the low dielectric polymer by the typically higher dielectric permittivity reaction mixture. Moreover, when using a dielectric permittivity value of 2 instead, roughly the value expected for an organic material, this approach reproduces IP and EA values measured experimentally for conjugated polymers by photoelectron spectroscopy,[2, 3] in which the polymer particles/film is measured in vacuum and there is no solvent/reaction mixture present.

The potentials of solution reactions, e.g., the reduction of CO_2 to formic acid or the reduction of protons to hydrogen, were calculated using a similar previously reported approach.[2, 3] In this case, just as for the polymer calculations, the solvent was assumed to be pure DMA. Moreover, in these solution potential calculations all soluble species are assumed to have a concentration of 1 mol/L, all gaseous species a pressure of 1 bar, and protons treated as adducts of a proton and the triethanolamine sacrificial electron donor ([H:TEAOH]+).

All DFT calculations used the B3LYP density functional[4-7] in combination with the DZP[8] basis-set and were performed using Turbomole 7.5..[9, 10] Solvation effects in the DFT calculations were described using the COSMO[11] implicit continuum solvation model and the DMA dielectric permittivity value discussed above.

All predicted potentials were converted from the vacuum scale to the standard hydrogen electrode (SHE) scale by subtracting 4.44 V, the absolute value of the standard hydrogen electrode potential, of the vacuum scale value. Approximate values of the predicted potentials vs. Fc were obtained by adding +0.6 V to the SHE values based on values reported in a literature[12] for MeCN, which has a similar dielectric constant as DMA.

The difference between the fundamental gap, itself the difference between the EA and IP (predicted by the DFT calculation to be 3.1 eV for P10) and the optical gap (experimentally measured to be 2.64 eV, Figure S1) can likely be rationalized by the strong exciton binding energy predicted for conjugated polymers. For instance, the experimentally measured exciton binding energies of many inorganic semiconductors are on the order of tens of meV, whilst the

magnitude of exciton binding energies for conjugated polymers are typically predicted to range from hundreds to thousands of meV.[13] The observed difference between the predicted fundamental gap and the observed optical gap of the polymers is consistent with this rationale.

Table S1 Predicted potentials for the conjugated polymers in DMA vs. SHE in V and in between parentheses their estimated approximate values vs. ferrocene.

	IP	EA
P1	0.92 (0.3)	-2.34 (-2.9)
P7	1.28 (0.7)	-1.82 (-2.4)
P10	1.46 (0.9)	-1.61 (-2.2)
P28	1.19 (0.6)	-1.61 (-2.2)

Table S2 Predicted solution reaction potentials in DMA vs. SHE in V and in between parentheses their estimated approximate values vs. ferrocene.

Half reaction	E
$TEAOH{:}H^+ + e^- \rightarrow \frac{1}{2} H_2$	-0.70 (-1.3)
$CO_2 + 2\ TEAOH{:}H^+ + 2\ e^- \rightarrow HCOOH + 2\ TEAOH$	-0.88 (-1.5)
$TEAOHR^{1} + TEAOH{:}H^+ + e^- \rightarrow 2\ TEAOH$	0.65 (0.1)

[1] TEAOHR is $N(CH_2CH_2OH)_2CHCH_2OH$

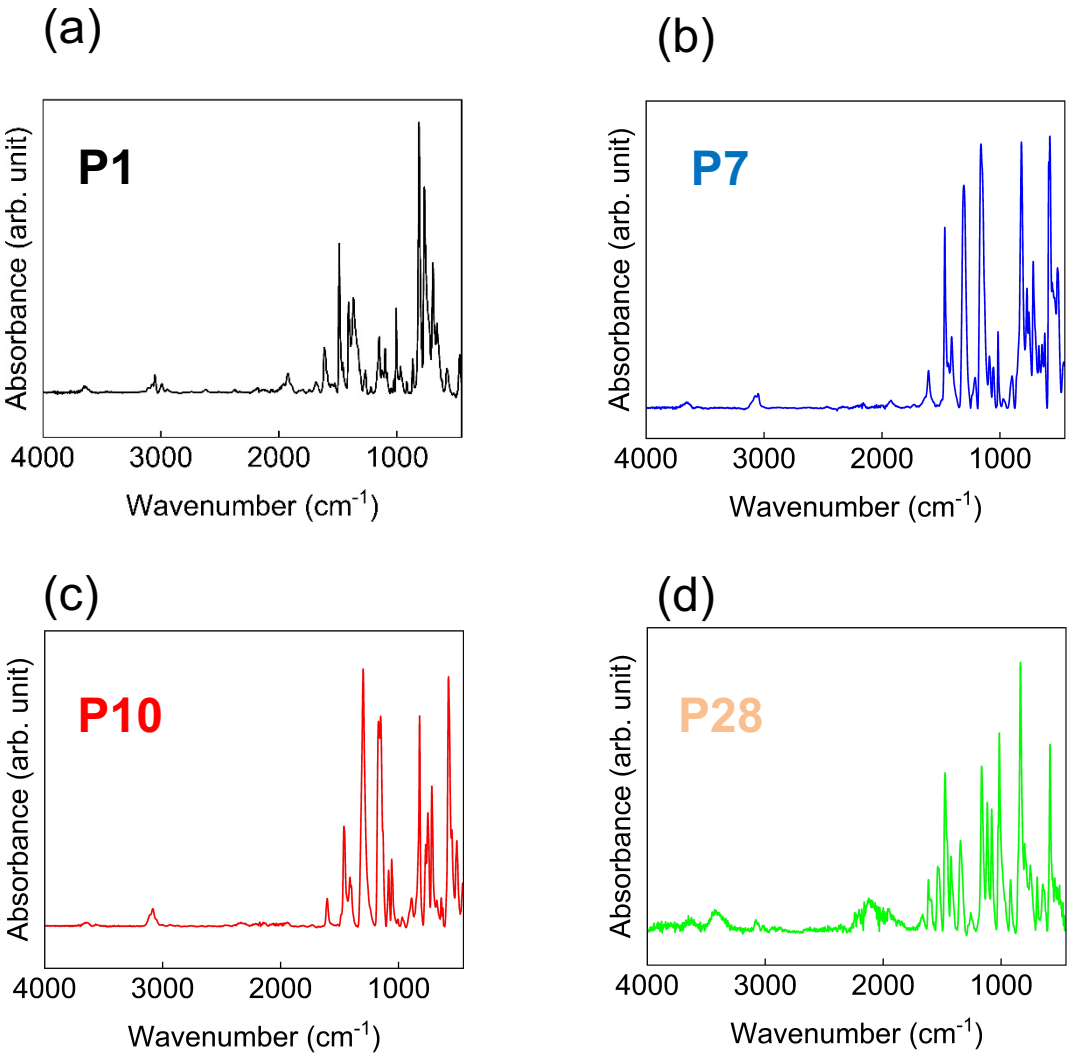

Figure S1 FT-IR spectra of (a) P1, (b) P7, (c) P10 and (d) P28.

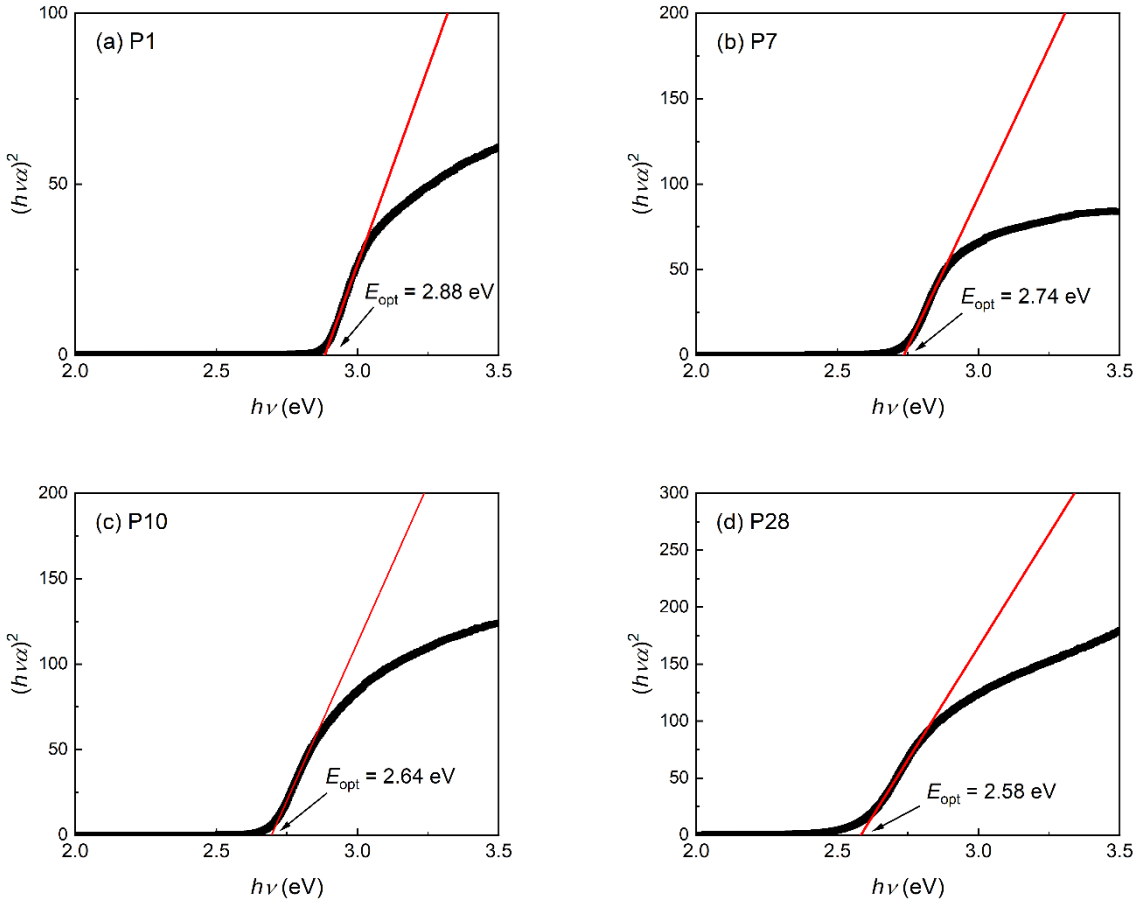

Figure S2 Tauc plot of (a) P1, (b) P7, (c) P10 and (d) P28.

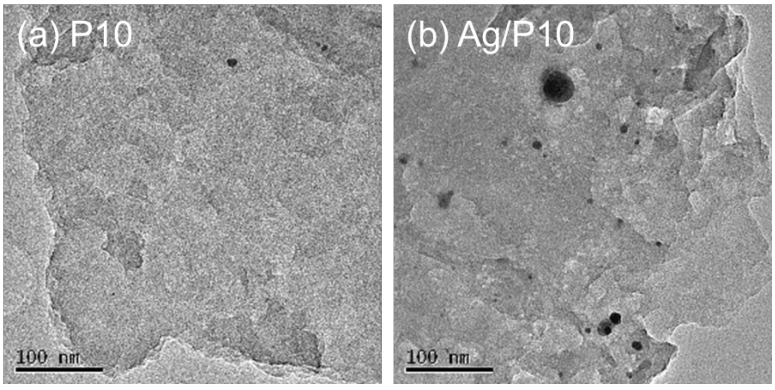

Figure S3 TEM images of (a) P10 and (b) Ag/P10 at 100 nm scale.

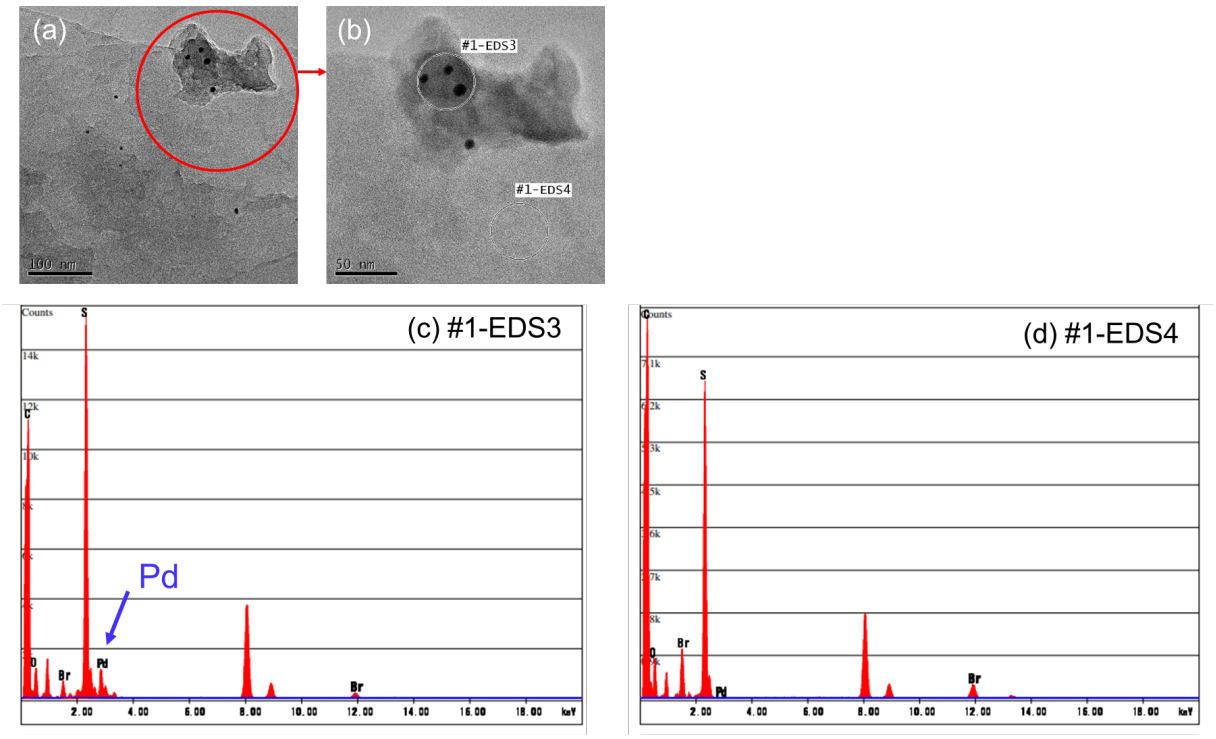

Figure S4 Transmission electron microscopy (TEM) images of P10 at (a) 100 nm and (b) 50 nm respectively, with the zoomed in regions highlighted by red circles. Regions marked EDS3 and EDS4 are circled with corresponding energy dispersive X-ray spectroscopy (EDS) data and atomic assignment (c) and (d) respectively.

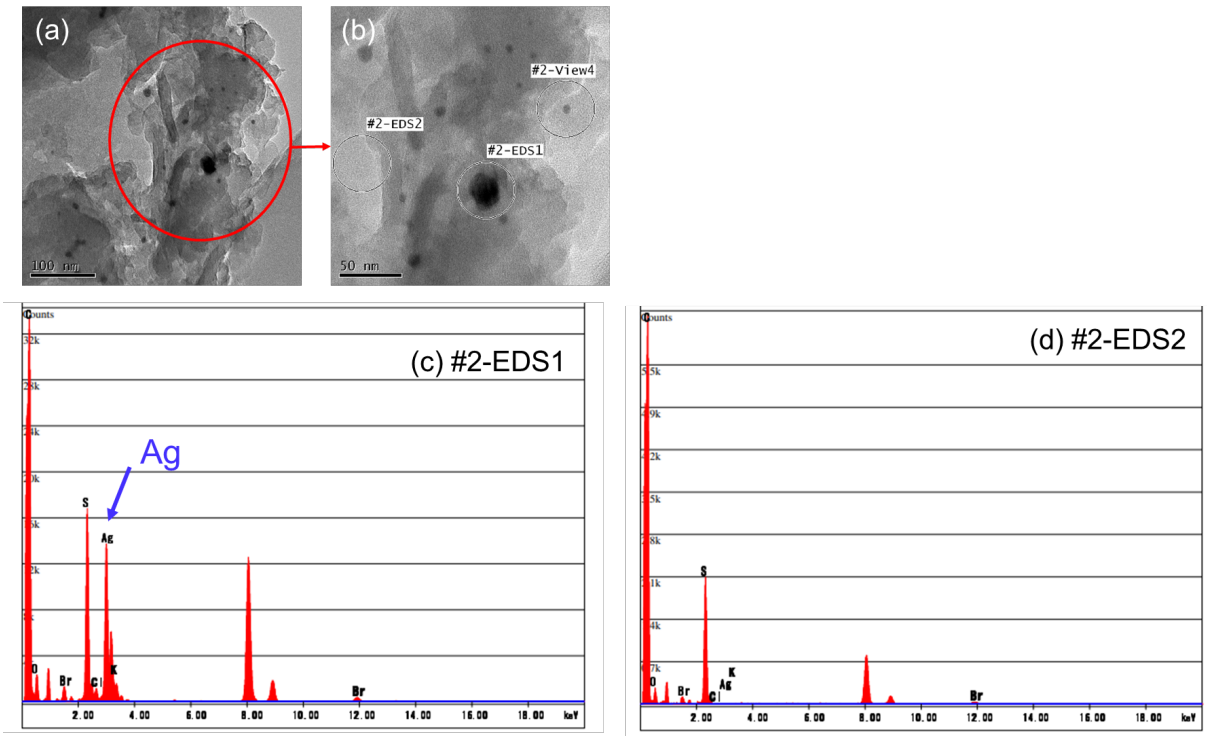

Figure S5 Transmission electron microscopy (TEM) images of Ag/P10 at (a) 100 nm and (b) 50 nm respectively, with the zoomed in regions highlighted by red circles. Regions marked EDS1 and EDS2 are circled with corresponding energy dispersive X-ray spectroscopy (EDS) data and atomic assignment (c) and (d) respectively.

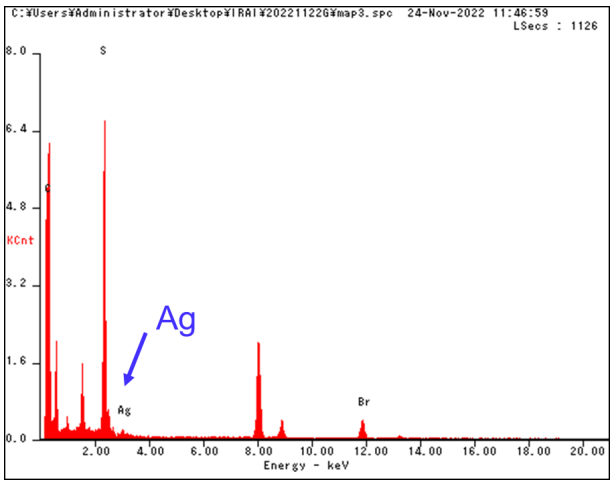

Figure S6 EDS spectrum of Ag/P10 corresponding to the EDS mapping analysis in Figure 3.

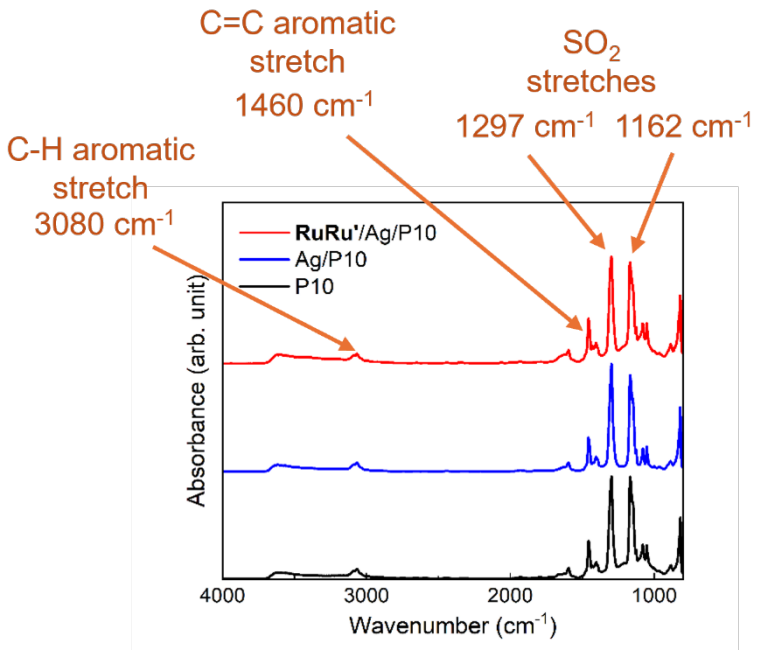

Figure S7 FT-IR spectra of P10, Ag/P10 and **RuRu'**/Ag/P10, corresponding to Figure 4a.

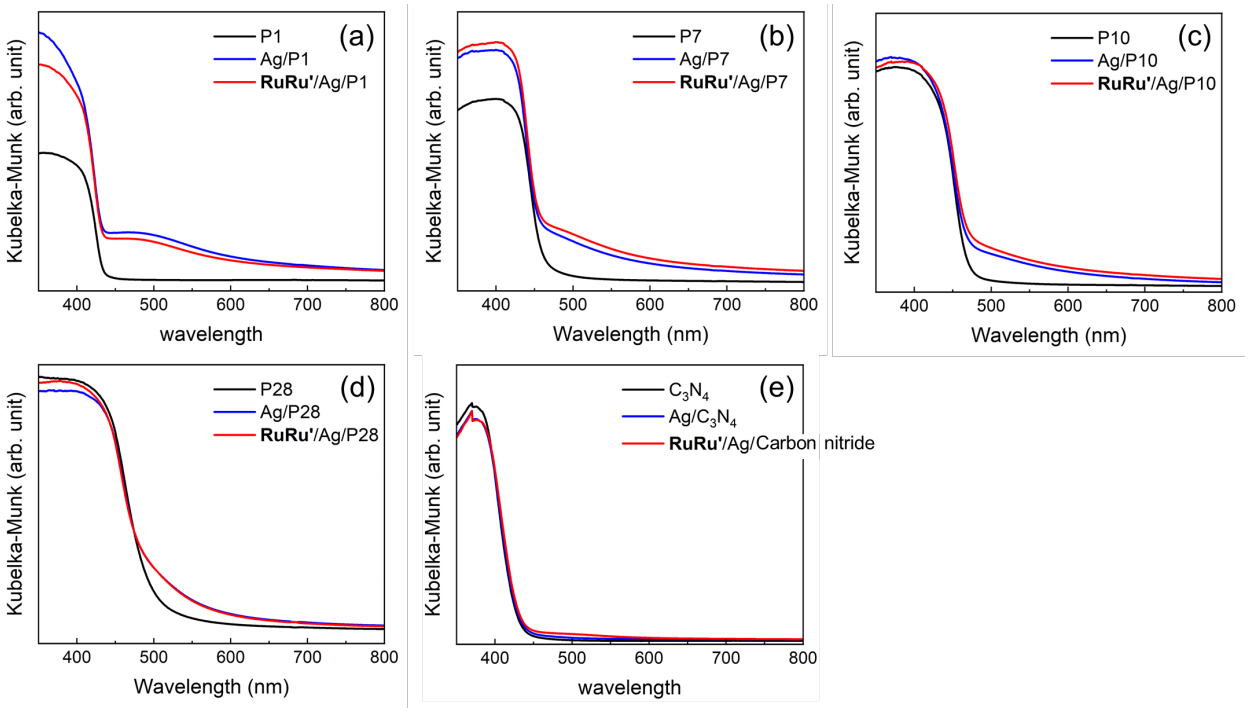

Figure S8 UV-diffuse reflectance spectra of (a) P1, (b) P7, (c) P10, (d) P28 and (e) carbon nitride, each overlaid with the UV-diffuse reflectance upon 1 wt.% silver loading and 0.4 μmol g^{-1} **RuRu'** adsorption.

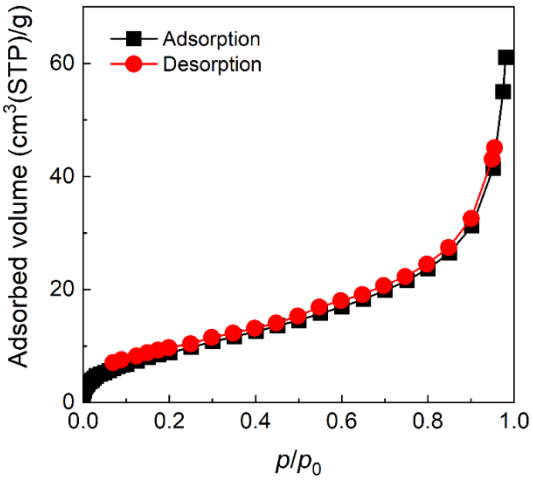

Figure S9 N_2 adsorption–desorption isotherm of P10 at 77 K.

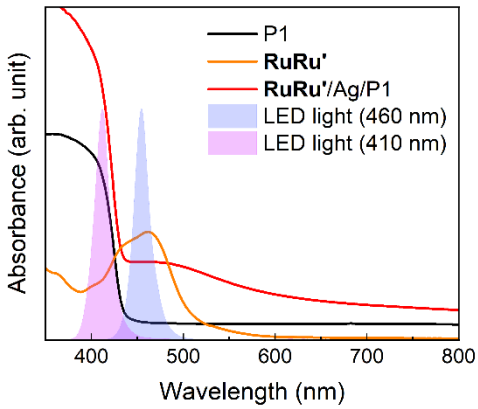

Figure S10 LED light spectra overlaid by spectra of P1, **RuRu'** and **RuRu'**/Ag/P1. 410 nm and 460 nm-LEDs were used for irradiation of **RuRu'**/Ag/P1 and **RuRu'**/Ag/carbon nitride.

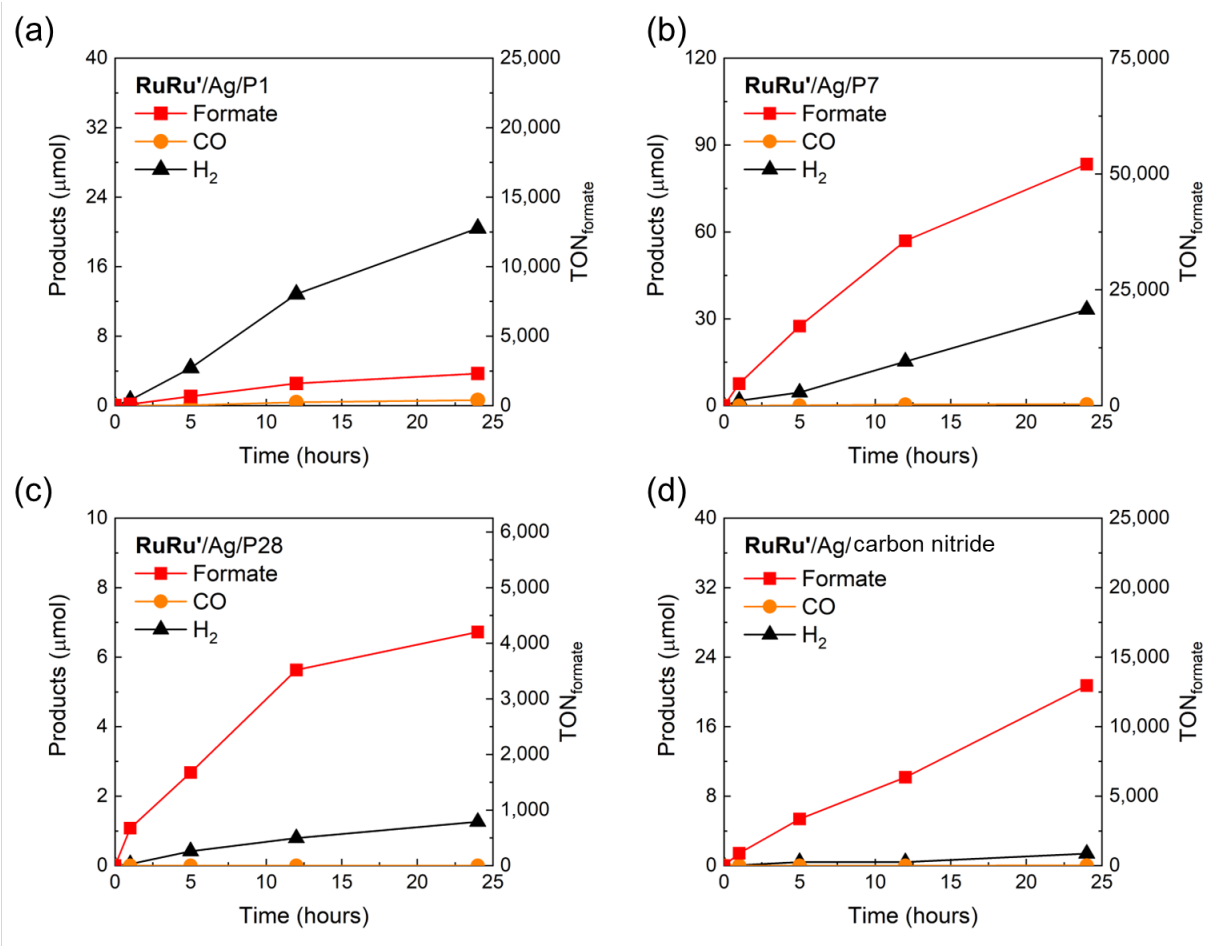

Figure S11 Total product formation during the photocatalytic reaction after 24 hours of irradiation using (a) **RuRu'** /Ag/P1, (b) **RuRu'** /Ag/P7, (c) **RuRu'** /Ag/P28 and (d) **RuRu'** /Ag/C_3N_4. Hybrid photocatalysts (4 mg, 1 wt.% Ag and 0.4 µmol g^{-1} **RuRu'** loading) were dispersed in 4 mL of DMA/TEOA (4:1), bubbled with CO_2 and irradiated using LED at 460 nm (with 5 mW output). For **RuRu'**/Ag/P1 and **RuRu'** /Ag/carbon nitride, additional light at 410 nm (with 5 mW output) was used. Note that the scale of the vertical axes are different amongst the graphs to aid the visibility.

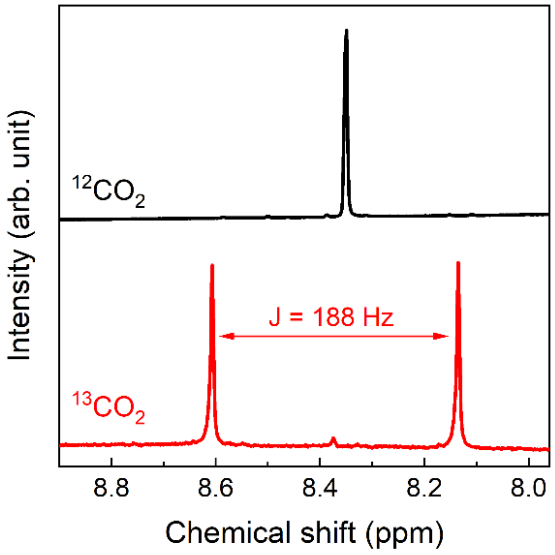

Figure S12 ^{1}H NMR spectra of DMA/TEOA solutions after the photocatalysis using **RuRu'**/Ag/P10. The photocatalyst powders were removed by filtration before the measurement. The suspension of **RuRu'**/Ag/P10 was irradiated by 460 nm LED for 24 hours under 640 mmHg of $^{13}CO_2$ (red) and saturated unlabeled CO_2 (black).

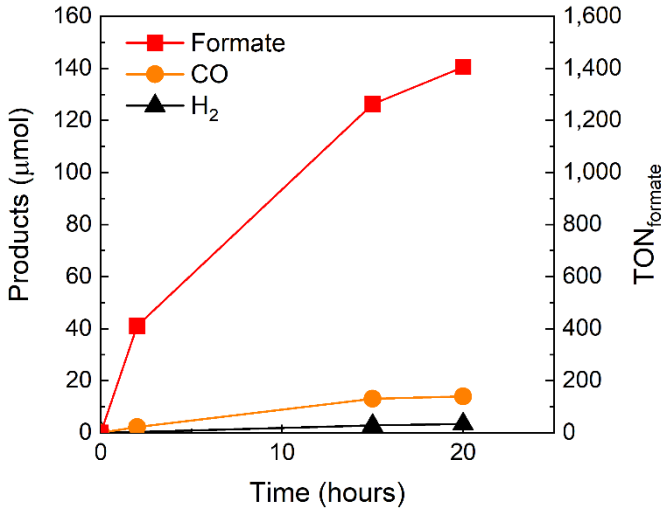

Figure S13 Time courses of products during the photocatalytic reactions in CO_2-saturated DMA solution (2 mL) containing dissolved **RuRu'** (0.05 mM) and BI(OH)H (0.2 M), which was irradiated using 460 nm-centered LED light source.

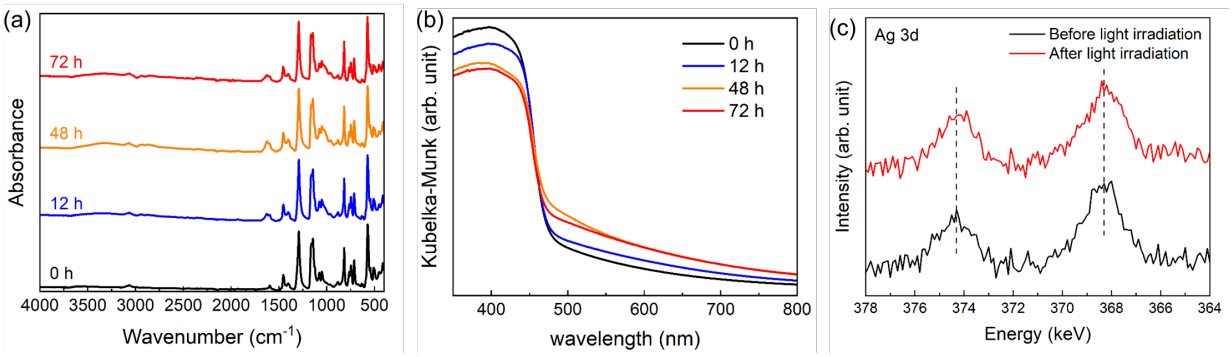

Figure S14 Characterization **RuRu'**/Ag/P10 before and after 12, 48 and 72 hours of light irradiation. (a) FTIR spectra. (b) UV-vis diffuse reflectance spectra. (c) Ag 3d XPS spectra before and after 72 hours light irradiation. For photocatalytic experiments, 1 mg of **RuRu'**/Ag/P10 was dispersed in 4 mL of 4:1 DMA/TEOA solution, thoroughly bubbled with CO_2 and irradiated at $\lambda = 460$ nm using an LED light source with constant stirring. The hybrid photocatalyst was washed with acetone and dried to be analyzed as a powder.

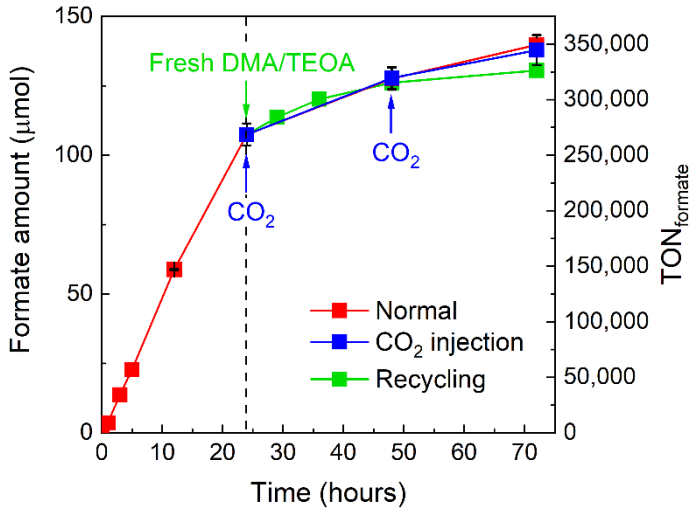

Figure S15 Temporal production of formic acid using **RuRu'**/Ag/P10 for photocatalytic CO_2 reduction (red trace, same conditions as described for Figure 7a), overlaid with measurements obtained with further CO_2 bubbling after 24 hours and 48 hours of photoirradiation (blue trace), and also overlaid with measurements obtained using fresh DMA/TEOA solution after 24 hours of photoirradiation (green trace).

Table S3. Apparent quantum yield (AQY) of hybrid photocatalysts composed of semiconductor and metal complexes reported thus far.

Entry	Hybrid photocatalyst[a]	Main product	Reported "AQY"[b] / %	Wavelength / nm	*A*	AQY (*A* = 1) / %	Reference
1	**RuRu'**/Ag/P10	HCOOH	11.2	440	1	11.2	**This study**
2	**Ru**/C_3N_4	HCOOH	5.7	400	2	2.9	[14]
3	**RuRu'**/Ag/C_3N_4	HCOOH	5.2	400	4	1.3	[15]
4	**Co**/ZnSe	CO	5.1	400	2	2.6	[16]
5	**Fe**/C_3N_4	CO	4.2	400	2	2.1	[17]
6	**Ru**/Ag/C_3N_4	HCOOH	4.2	400	2	2.1	[18]
7	**Ni**/ZnSe-QD	CO	3.4	400	2	1.7	[19]
8	**Zn**/TiO_2/**Re**	CO	3.21	436	2	1.6	[20]
9	**Ru**/Ag/CNU	HCOOH	3.1	400	2	1.6	[21]
10	**RuRe**/C_3N_4	CO	2.5	400	4	0.6	[22]
11	**Re**/Dye/TiO_2	CO	2.14	436	2	1.1	[23]
12	**Re**/Zn-Porphyrinic-MOF	CO	1.97	440	1	1.97	[24]
13	**Ru**/N-Ta_2O_5	HCOOH	1.9	405	2	1.0	[25]
14	**Co**/C_3N_4	CO	1.6	420	2	0.8	[26]
15	**RuRu'**/Ag/C_3N_4	HCOOH	1.6	400	4	0.4	[27]
16	**Ru**/C_3N_4	HCOOH	1.5	400	2	0.8	[28]
17	**Ru**/C_3N_4	HCOOH	1.1	400	2	0.6	[29]
18	**RuRu'**/Ag/GaN:ZnO	HCOOH	1.0	400	4	0.3	[30]
19	**RuRe**/TiO_2/C_3N_4	CO	0.6	400	4	0.2	[31]
20	**Re**/COF	CO	0.5	420	2	0.3	[32]
21	**RuRu'**/Ag/TaON	HCOOH	0.48	400	1	0.48	[33]
22	**Re**, **Co**/Dye/TiO_2	CO	0.46	420–450	2	0.2	[34]
23	**Ru**/Cz-bpy	HCOOH	0.44	505	2	0.2	[35]
24	**Co**/C_3N_4	CO	0.25	400	2	0.1	[36]
25	**Ni**/$CsPbBr_3$	CO, CH_4	0.24	450	1	0.23	[37]
26	**Co**/C_3N_4	CO	0.11	360	2	0.05	[38]
27	**Fe**/C_3N_4	CO	0.10	460	2	0.05	[39]
28	**Re**/Zn-Porphyrinic-MOF	CO	0.10	450	2	0.05	[40]

[a] In the description of each hybrid photocatalyst, the metal complex catalyst is described in bold. [b] In many other reports, AQY is defined as follows: AQY = A×(total number of products) / (total number of incident photons).[41] For two-electron CO_2 reduction, A = 2 as the maximum AQY becomes 100%, which allows easy understanding of reaction efficiency of the photocatalytic system. However, when considering the initial meaning of quantum yield as a conversion efficiency of photons, A = 1 is suitable as a coefficient for quantum yield in these systems because of the complexities associated with the possible reaction mechanisms of photocatalytic CO_2 reduction as described in detail in the Apparent quantum yield measurements section in Methods. Thus, the AQY values were recalculated using A =1, listed in this table as AQY (A = 1).

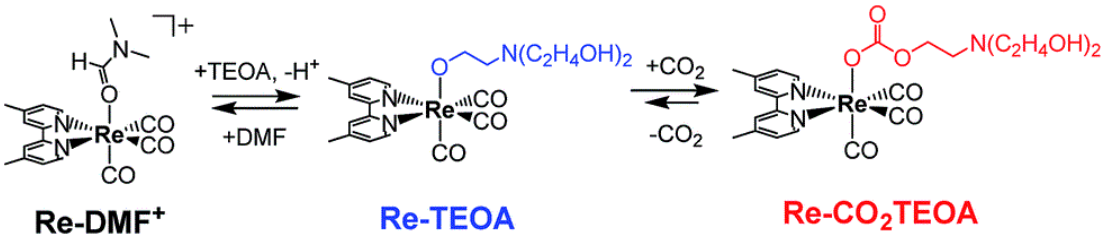

Scheme S1. Ligand substitution by TEOA and CO_2 capture into the Re(I) complex catalyst. Reproduced with permission from ref [42]. Copyright 2019 Royal Society of Chemistry.

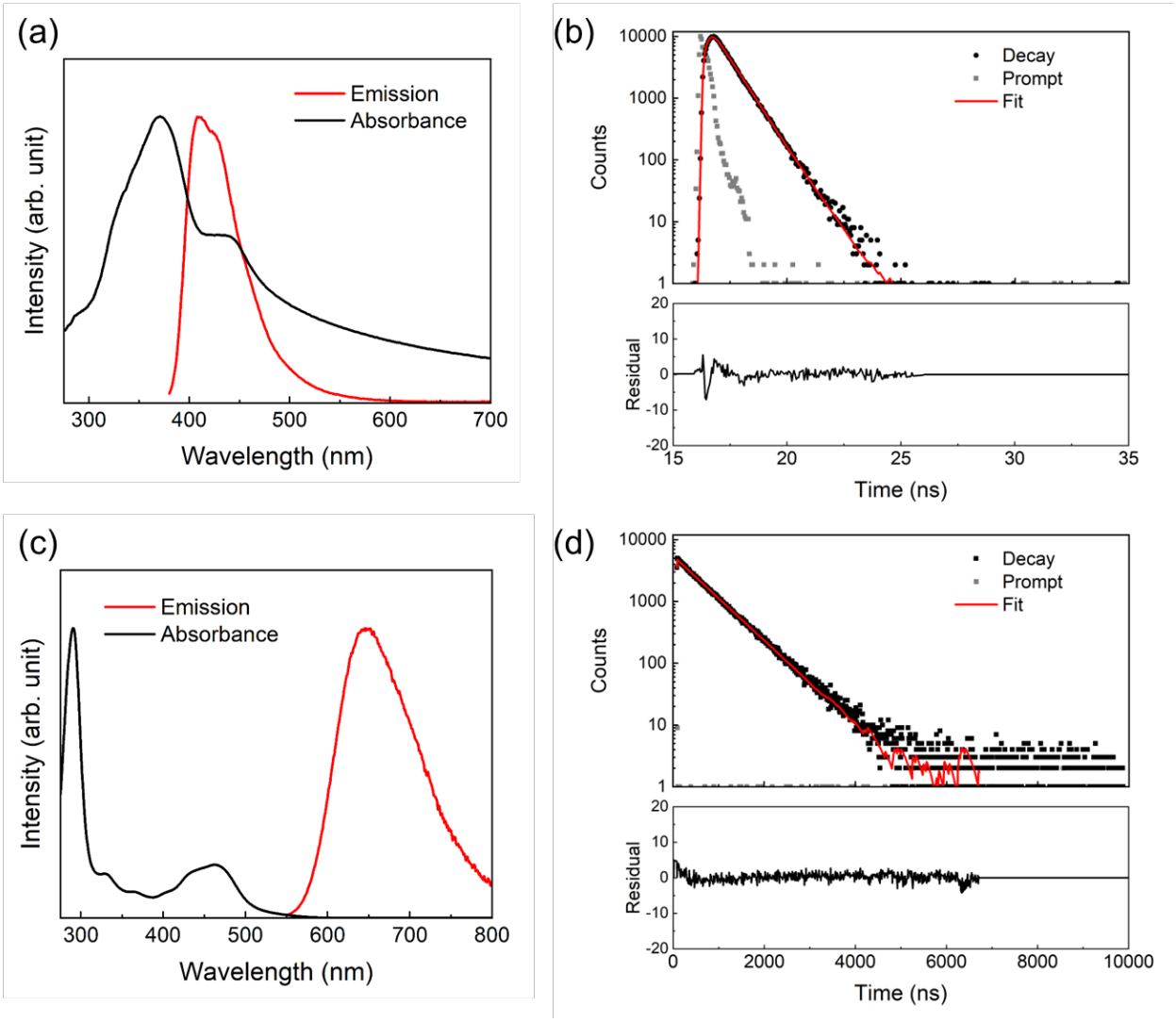

Figure S16 Absorbance and Photoluminescence spectra of (a) P10 and (c) **Ru(PS)** and emission decays of (b) P10 and (d) **Ru(PS)** in DMA solution. Photoluminescence spectra were obtained by the excitation at 370 nm and 460 nm for P10 and **Ru(PS)**, respectively. Emission decays are obtained by the excitation at 379 nm and emission at 410 nm for P10 and by the excitation at 456 nm and emission at 650 nm for **Ru(PS)**. The emission decays are fitted by exponential fitting with lifetimes measured as 0.81 ns for P10 and 615 ns for **Ru(PS)**.

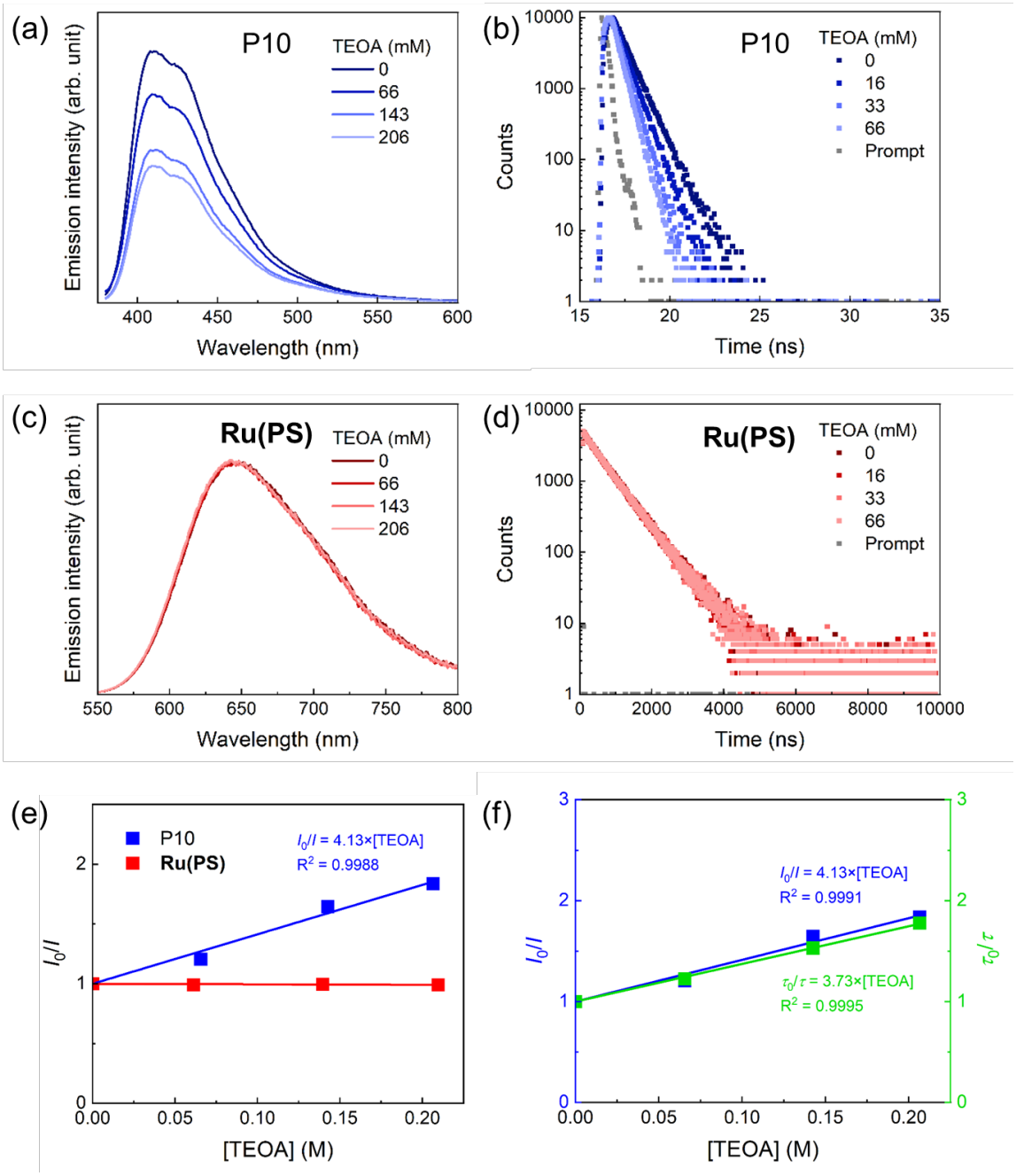

Figure S17 Emission quenching studies of P10 and **Ru(PS)** by TEOA in DMA solution. Photoluminescence emission spectra and its quenching by TEOA for (a) P10 and (c) **Ru(PS)**, emission decays corresponding to the emission quenching for (b) P10 and (d) **Ru(PS)**, and (e) Stern-Volmer plots of P10 and Ru(PS) obtained from the emission quenching by TEOA. (f) The Stern-Volmer plot of P10 obtained from the emission lifetimes with TEOA was in good agreement with that obtained from the emission quenching. The excitation and emission wavelengths for the measurements were the same as those used in Figure S15.

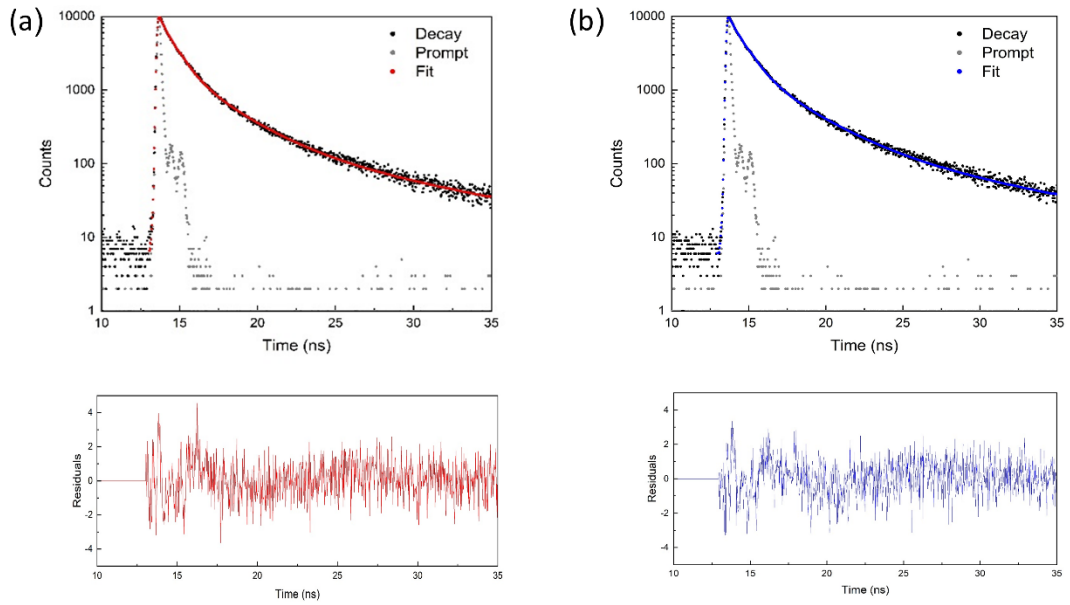

Sample	B_1	τ_1 (ns)	B_2	τ_2 (ns)	B_3	τ_3 (ns)	χ^2	Average weighted fluorescence lifetime (ns)
P10	0.02471256 (40.72%)	2.575837	0.002786022 (16.56%)	9.291161	0.08837704 (42.72%)	0.7556359	1.180261	**1.35**
Ag/P10	0.02391391 (40.45%)	2.856008	0.002620343 (15.41%)	9.92927	0.08990866 (44.13%)	0.8285727	1.201916	**1.45**

Figure S18 (a) Time resolved single photon counting (TRSPC) measurements of P10 (red) and (b) Ag/P10 (blue) in a sonicated suspension of DMA with the corresponding residuals plotted underneath. Emission lifetime decays are plotted along with the prompt and fitting. Initial excitation at 374 nm was used and emitted photons at 525 nm were detected in accordance with the emission spectrum. Estimated weighted average lifetimes of the excited states corresponding to P10 and Ag/P10 are also tabulated underneath. The emission lifetime was calculated using three exponentials by the following equation: $B_1 \times \exp(-i/\tau_1) + B_2 \times \exp(-i/\tau_2) + B_3 \times \exp(-i/\tau_3)$. Amplitudes ($B_1$, B_2 and B_3) are estimated and iterated along with the lifetimes (τ_1, τ_2 and τ_3) until a fit is found. The prompt was measured separately and used for deconvolution of the instrument response.

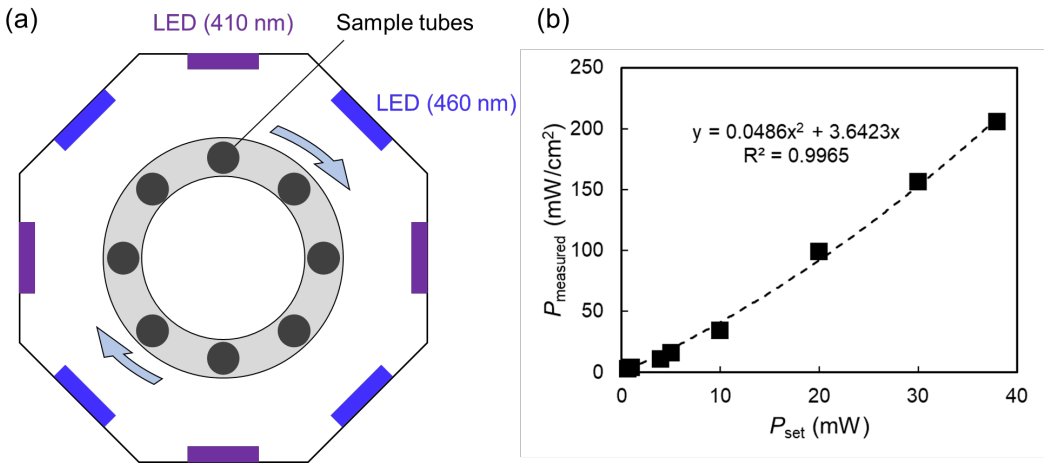

Figure S19 (a) Schematic illustration of the Iris-MG (CELL System Co.) light irradiation system with LEDs. Four LEDs with 460 nm and four LEDs with 410 nm are equipped. Sample tubes for photocatalytic experiments are set in the circular positions and the tubes are rotated around in a circle for uniform irradiation. The reaction solution was stirred continuously by a stirrer in the sample tube. (b) The relationship between the set values of LED output (P_{set}) and the light intensity of one LED measured on its surface ($P_{measured}$). One LED has the area of 2 cm^2. The output values in the manuscript are described as LED output values (P_{set}).

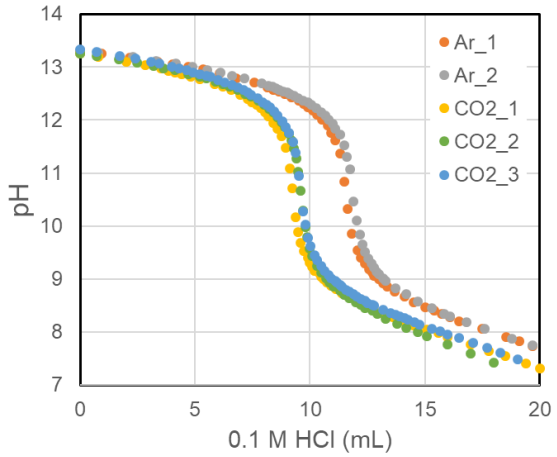

Figure S20 Counter titration plots for estimating saturated-CO_2 concentration in DMA/TEOA (4:1, v/v). The counter titration plots were obtained both in Ar and CO_2 atmosphere. The saturation concentration of CO_2 in the solution was estimated from the difference in the titration points.

References

1. P. Guiglion, C. Butchosa and M. A. Zwijnenburg, *J. Mater. Chem. A*, 2014, **2**, 11996-12004.
2. P. Guiglion, A. Monti and M. A. Zwijnenburg, *J. Phys. Chem. C*, 2017, **121**, 1498-1506.
3. D. J. Woods, S. A. J. Hillman, D. Pearce, L. Wilbraham, L. Q. Flagg, W. Duffy, I. McCulloch, J. R. Durrant, A. A. Y. Guilbert, M. A. Zwijnenburg, R. S. Sprick, J. Nelson and A. I. Cooper, *Energy Environ. Sci.*, 2020, **13**, 1843-1855.
4. A. D. Becke, *J. Chem. Phys.*, 1993, **98**, 5648-5652.
5. C. Lee, W. Yang and R. G. Parr, *Phys. Rev. B*, 1988, **37**, 785-789.
6. S. H. Vosko, L. Wilk and M. Nusair, *Can. J. Phys.*, 1980, **58**, 1200-1211.
7. P. J. Stephens, F. J. Devlin, C. F. Chabalowski and M. J. Frisch, *J. Phys. Chem.*, 1994, **98**, 11623-11627.
8. A. Schäfer, H. Horn and R. Ahlrichs, *J. Chem. Phys.*, 1992, **97**, 2571-2577.
9. F. Furche, R. Ahlrichs, C. Hättig, W. Klopper, M. Sierka and F. Weigend, *WIREs Comput. Mol. Sci.*, 2014, **4**, 91-100.
10. S. G. Balasubramani, G. P. Chen, S. Coriani, M. Diedenhofen, M. S. Frank, Y. J. Franzke, F. Furche, R. Grotjahn, M. E. Harding, C. Hättig, A. Hellweg, B. Helmich-Paris, C. Holzer, U. Huniar, M. Kaupp, A. Marefat Khah, S. Karbalaei Khani, T. Müller, F. Mack, B. D. Nguyen, S. M. Parker, E. Perlt, D. Rappoport, K. Reiter, S. Roy, M. Rückert, G. Schmitz, M. Sierka, E. Tapavicza, D. P. Tew, C. van Wüllen, V. K. Voora, F. Weigend, A. Wodyński and J. M. Yu, *J. Chem. Phys.*, 2020, **152**.
11. A. Klamt and G. Schüürmann, *J. Chem. Soc., Perkin Trans. 2*, 1993, DOI: 10.1039/P29930000799, 799-805.
12. N. G. Connelly and W. E. Geiger, *Chem. Rev.*, 1996, **96**, 877-910.
13. P. Guiglion, C. Butchosa and M. A. Zwijnenburg, *Macromol. Chem. Phys.*, 2016, **217**, 344-353.
14. R. Kuriki, K. Sekizawa, O. Ishitani and K. Maeda, *Angew. Chem. Int. Ed.*, 2015, **54**, 2406-2409.
15. R. Kuriki, H. Matsunaga, T. Nakashima, K. Wada, A. Yamakata, O. Ishitani and K. Maeda, *J. Am. Chem. Soc.*, 2016, **138**, 5159-5170.
16. C. D. Sahm, G. M. Ucoski, S. Roy and E. Reisner, *ACS Catal.*, 2021, **11**, 11266-11277.
17. C. Cometto, R. Kuriki, L. Chen, K. Maeda, T.-C. Lau, O. Ishitani and M. Robert, *J. Am. Chem. Soc.*, 2018, **140**, 7437-7440.
18. K. Maeda, D. An, C. S. Kumara Ranasinghe, T. Uchiyama, R. Kuriki, T. Kanazawa, D. Lu, S. Nozawa, A. Yamakata, Y. Uchimoto and O. Ishitani, *J. Mater. Chem. A*, 2018, **6**, 9708-9715.
19. M. F. Kuehnel, C. D. Sahm, G. Neri, J. R. Lee, Katherine L. Orchard, A. J. Cowan and E. Reisner, *Chem. Sci.*, 2018, **9**, 2501-2509.
20. D.-I. Won, J.-S. Lee, Q. Ba, Y.-J. Cho, H.-Y. Cheong, S. Choi, C. H. Kim, H.-J. Son, C. Pac and S. O. Kang, *ACS Catal.*, 2018, **8**, 1018-1030.
21. K. Shibata, K. Kato, C. Tsounis, T. Kanazawa, D. Lu, S. Nozawa, A. Yamakata, O. Ishitani and K. Maeda, *Solar RRL*, 2020, **4**, 1900461.
22. K. Wada, M. Eguchi, O. Ishitani and K. Maeda, *ChemSusChem*, 2017, **10**, 287-295.

23. D.-I. Won, J.-S. Lee, J.-M. Ji, W.-J. Jung, H.-J. Son, C. Pac and S. O. Kang, *J. Am. Chem. Soc.*, 2015, **137**, 13679-13690.
24. S. Choi, W.-J. Jung, K. Park, S.-Y. Kim, J.-O. Baeg, C. H. Kim, H.-J. Son, C. Pac and S. O. Kang, *ACS Appl. Mater. Interfaces*, 2021, **13**, 2710-2722.
25. S. Sato, T. Morikawa, S. Saeki, T. Kajino and T. Motohiro, *Angew. Chem. Int. Ed.*, 2010, **49**, 5101-5105.
26. J. J. Walsh, C. Jiang, J. Tang and A. J. Cowan, *Phys. Chem. Chem. Phys.*, 2016, **18**, 24825-24829.
27. N. Sakakibara, M. Shizuno, T. Kanazawa, K. Kato, A. Yamakata, S. Nozawa, T. Ito, K. Terashima, K. Maeda, Y. Tamaki and O. Ishitani, *ACS Appl. Mater. Interfaces*, 2023, **15**, 13205-13218.
28. K. Maeda, K. Sekizawa and O. Ishitani, *Chem. Commun.*, 2013, **49**, 10127-10129.
29. C. Tsounis, R. Kuriki, K. Shibata, J. J. M. Vequizo, D. Lu, A. Yamakata, O. Ishitani, R. Amal and K. Maeda, *ACS Sustainable Chem. Eng.*, 2018, **6**, 15333-15340.
30. A. Nakada, R. Kuriki, K. Sekizawa, S. Nishioka, J. J. M. Vequizo, T. Uchiyama, N. Kawakami, D. Lu, A. Yamakata, Y. Uchimoto, O. Ishitani and K. Maeda, *ACS Catal.*, 2018, **8**, 9744-9754.
31. K. Wada, C. S. K. Ranasinghe, R. Kuriki, A. Yamakata, O. Ishitani and K. Maeda, *ACS Appl. Mater. Interfaces*, 2017, **9**, 23869-23877.
32. Z. Fu, X. Wang, A. M. Gardner, X. Wang, S. Y. Chong, G. Neri, A. J. Cowan, L. Liu, X. Li, A. Vogel, R. Clowes, M. Bilton, L. Chen, R. S. Sprick and A. I. Cooper, *Chem. Sci.*, 2020, **11**, 543-550.
33. A. Nakada, T. Nakashima, K. Sekizawa, K. Maeda and O. Ishitani, *Chem. Sci.*, 2016, **7**, 4364-4371.
34. J.-S. Lee, D.-I. Won, W.-J. Jung, H.-J. Son, C. Pac and S. O. Kang, *Angew. Chem. Int. Ed.*, 2017, **56**, 976-980.
35. A. Nakada, R. Miyakawa, R. Itagaki, K. Kato, C. Takashima, A. Saeki, A. Yamakata, R. Abe, H. Nakai and H.-C. Chang, *J. Mater. Chem. A*, 2022, **10**, 19821-19828.
36. B. Ma, G. Chen, C. Fave, L. Chen, R. Kuriki, K. Maeda, O. Ishitani, T.-C. Lau, J. Bonin and M. Robert, *J. Am. Chem. Soc.*, 2020, **142**, 6188-6195.
37. Z. Chen, Y. Hu, J. Wang, Q. Shen, Y. Zhang, C. Ding, Y. Bai, G. Jiang, Z. Li and N. Gaponik, *Chem. Mater.*, 2020, **32**, 1517-1525.
38. S. Roy and E. Reisner, *Angew. Chem. Int. Ed.*, 2019, **58**, 12180-12184.
39. Y. Wei, L. Chen, H. Chen, L. Cai, G. Tan, Y. Qiu, Q. Xiang, G. Chen, T.-C. Lau and M. Robert, *Angew. Chem. Int. Ed.*, 2022, **61**, e202116832.
40. P. M. Stanley, K. Hemmer, M. Hegelmann, A. Schulz, M. Park, M. Elsner, M. Cokoja and J. Warnan, *Chem. Sci.*, 2022, **13**, 12164-12174.
41. A. J. Morris, G. J. Meyer and E. Fujita, *Acc. Chem. Res.*, 2009, **42**, 1983-1994.
42. H. Kumagai, T. Nishikawa, H. Koizumi, T. Yatsu, G. Sahara, Y. Yamazaki, Y. Tamaki and O. Ishitani, *Chem. Sci.*, 2019, **10**, 1597-1606.